

Enhanced Open-Circuit Voltage of Wide-Bandgap Perovskite Photovoltaics by Using Alloyed $(\text{FA}_{1-x}\text{Cs}_x)\text{Pb}(\text{I}_{1-x}\text{Br}_x)_3$ Quantum Dots

Mokshin Suri,^{†,‡} Abhijit Hazarika,[†] Bryon Larson,[†] Qian Zhao,^{†,§} Marta Vallés-Pelarda,^{||,†} Timothy D. Siegler,[‡] Michael K. Abney,[‡] Andrew J. Ferguson,[†] Brian A. Korgel,^{‡,*} and Joseph M. Luther^{†,*}

[†] National Renewable Energy Laboratory, Golden, Colorado 80401, USA

[‡] McKetta Department of Chemical Engineering and Texas Materials Institute, The University of Texas at Austin, Austin, Texas 78712-1062, USA

[§] College of Chemistry, Nankai University, Tianjin 300071, China

^{||} Institute of Advanced Materials (INAM), Universitat Jaume I, Avenida de Vicent Sos Baynat, s/n, 12006 Castelló de la Plana, Castellón, Spain

* Corresponding authors: joey.luther@nrel.gov; korgel@che.utexas.edu

SUPPORTING INFORMATION

- Experimental Methods
- Characterizations
- Figure S1. Comparison of experimental PQD PV voltage fractions to literature
- Table S1. Device metrics of PQD PVs used in Fig. 2 of main text.
- Figure S2. Radiative lifetime estimates of all colloidal PQD samples
- Figure S3. TRPL transients of all PQD samples
- Table S2. Fitting parameters of time-resolved PL decays in Figure S3.
- Table S3. Device metrics of all PQD PVs, from Fig. 4 of main text
- Figure S4. Time-resolved microwave conductivity (TRMC) of PQD films.
- Figure S5. Yield-mobility product of PQD films
- Figure S6. Absorbance and photoluminescence of $\text{CsPb}(\text{I}_{1-x}\text{Br}_x)_3$ PQD samples used in devices and TRMC measurements.
- Figure S7. Absorbance and photoluminescence of $\text{FAPb}(\text{I}_{1-x}\text{Br}_x)_3$ PQD samples used in devices and TRMC measurements.

Experimental Methods

Chemicals

All chemicals were used as received without further purification. Oleic acid (OA, technical grade 90%), oleylamine (OAm, technical grade 70%), 1-octadecene (ODE, technical grade 90%), toluene (anhydrous, 99.8%), hexane (reagent grade $\geq 95\%$), octane (anhydrous, $\geq 99\%$), 1-butanol (anhydrous, 99.8%), methyl acetate (MeOAc, anhydrous 99.5%), ethyl acetate (EtOAc, anhydrous, 99.8%), cesium carbonate (Cs_2CO_3 , 99.9%), lead (II) nitrate ($\text{Pb}(\text{NO}_3)_2$, 99.999%), ethanol (EtOH, 200 proof), titanium ethoxide ($>97\%$), hydrochloric acid (HCl; 37% in water), chlorobenzene (anhydrous, 99.8%), 4-tert-butylpyridine (4-TBP, 96%), bis(trifluoromethane)sulfonimide lithium salt (Li-TFSI, 99.95% trace metals basis), Formamidinium acetate salt (FA-acetate, 99%), and acetonitrile (anhydrous, 99.8%) were purchased from Sigma-Aldrich. Lead (II) iodide (PbI_2 99.9985%) was purchased from Alfa Aesar. Formamidinium iodide (FAI) was purchased from GreatCell Solar. 2,2',7,7'-Tetrakis(N,N-di-p-methoxyphenylamine)-9-9'-spirobifluorene (spiro-OMeTAD, $\geq 99.5\%$) was purchased from Lumtech, Inc.

Syntheses of perovskite QDs

CsPb(I_{1-x}Br_x)₃ QD synthesis

1.08 mmol of PbX_2 powder (mixture of PbI_2 and PbBr_2) was dissolved in octadecene in a 3-neck flask. The mixture was subjected to a vacuum environment and heated to 110 °C for 10 minutes. 2.5 mL of oleylamine and 2.5 mL oleic acid were heated to 130 °C and injected into the flask. This allows for dissolution of the lead salt; once the salt dissolves, the flask was subjected to a nitrogen environment and the solution was heated to 185 °C. As soon as the solution temperature reached 185 °C, a Cs-oleate precursor, at 130 °C, was injected all at once into the flask. This procedure is adapted from previous reports.^{1,2}

The Cs-oleate precursor was created by dissolving 407 mg of Cs_2CO_3 in 20 mL of octadecene and 1.25 mL of oleic acid. Proper dissolution of the Cs-oleate required degassing at 120 °C followed by heating to 150 °C.

Nucleation of CsPbX_3 quantum dots occurs nearly instantaneously as the Cs-oleate is injected into the lead salt solution. In order to maintain relative mono-dispersity of the quantum dots, the flask was cooled to 25-30 °C in an ice bath immediately following injection of the Cs-oleate.

Extra ligands were removed from the quantum dot solution by centrifuging with anhydrous methyl acetate for 5 minutes at 7500 RPM. Multiple washing steps were required to produce high yield product.²

FAPb(I_{1-x}Br_x)₃ QD synthesis

0.74 mmol of PbX_2 powder (mixture of PbI_2 and PbBr_2) were mixed in 25 mL of octadecene in a 3-neck flask. The mixture was degassed for 20 minutes at 120 °C. Separately, 4mL of oleic acid and 2mL of oleylamine were mixed at 130 °C for 20 min. The oleic acid/oleylamine mixture

was then injected into the Pb-salt flask to dissolve the Pb-salt. Once the salts dissolved, the flask atmosphere was changed to nitrogen and the temperature was adjusted to a targeted reaction temperature depending on input halide ratio of the lead-salts.

Separately, FA-oleate precursor was prepared by mixing 521 mg of FA-acetate in 10-20 mL oleic acid in a 3-neck flask, yielding a FA concentration of 0.25-0.50 mM. The concentration of FA-acetate used for this synthesis varied linearly from 0.25-0.50 mM based on input molar halide ratio of the PbX_2 salts. For $FAPbI_3$, 0.50 mM of FA-acetate was used, and for $FAPbBr_3$, 0.25 mM of FA-acetate was used. This solution was then degassed at 50 °C for 20 minutes, after which, the temperature was increased to 120 °C to induce complete dissolution of the FA-oleate.^{3,4} Once dissolved, the atmosphere of the 3-neck flask was changed to nitrogen before the injection process.

The reaction temperature to form $FAPb(I_{1-x}Br_x)_3$ QDs varied from linearly 80 °C-135 °C based on input molar halide composition, with $FAPbBr_3$ synthesis occurring at 135 °C and $FAPbI_3$ at 80 °C. 5-10 mL of the FA-oleate precursor was rapidly injected into the PbX_2 solution at a targeted temperature and the reaction flask was quickly quenched in an ice bath. (The concentration of FA-oleate was different based on halide ratio, however, an equal molar amount of FA-oleate was injected across all halide ratios. Typically, the input molar halide ratio of the PbX_2 salts varied by 10-20% from the molar halide ratio of the final product.)

To remove excess ligands, the QDs were taken into 3 mL of toluene and then subsequently crashed out of solution by adding 5 mL of methyl acetate to the toluene suspension and centrifuging at 8000 RPM for 30 minutes. The supernatant was discarded and the resulting pellet was dispersed in 7 mL of toluene. The toluene based QD solution was mixed with 5mL of methyl acetate and centrifuged at 8000 RPM for 10 minutes. The resulting supernatant was discarded and the pellet was dispersed in octane for use in characterization and device fabrication.

$FA_{1-x}Cs_xPb(I_{1-x}Br_x)_3$ QD synthesis

Mixed A-site QDs were formed via post-synthetic mixing using methods similar to those shown by Hazarika et.al.⁴ First, $FAPbI_3$ and $CsPbBr_3$ QDs were synthesized using the methods outlined above. Then, $FAPbI_3$ and $CsPbBr_3$ QD solutions were mixed at 70°C for 24 hours in a fixed Cs:FA molar ratio. To confirm the existence of single phase $FA_{1-x}Cs_xPb(I_{1-x}Br_x)_3$ QDs, the resultant nanocrystals were characterized via photoluminescence emission and UV-Vis-NIR absorbance spectroscopy to ensure the convergence of the luminescence peak and first exciton.

Characterizations

Absorbance and Photoluminescence

UV-Vis absorption spectra were measured using a Shimadzu UV-3600 UV-VIS-NIR absorption spectrophotometer. Steady state PL emissions and PL excitation spectra were measured in a Horiba's Fluoromax-4 emission spectrophotometer.

QD film fabrication for devices and TRMC measurements

QD films were fabricated based on previously reported methods.⁵ Saturated solutions of $Pb(NO_3)_2$ in MeOAc and FAI in EtOAc were prepared. Excess salt was removed by centrifugation at 3500

RPM for 5 min. To prepare the QD film, concentrated QD solutions (~75 mg/mL) were spin-cast onto a TiO₂ surface at 1000 RPM for 20 s followed by 2000 RPM for 5 s. The resulting films were dipped into the Pb(NO₃)₂ solution for ~3 s followed by rinsing with neat MeOAc for ~3 s. This process was repeated 3 times to produce a thick QD film (100-400 nm). During the ligand exchange with the Pb(NO₃)₂ solution, the ambient relative humidity (RH) was held at 15-25% RH in a climate controlled glovebox. Once a thick QD film was deposited, ambient humidity was reduced to 0% RH, and the films were post-treated with the FAI solution. The films were dipped into the FAI solution for 10 s followed by rinsing with neat MeOAc.

Device fabrication

A 50nm layer of TiO₂ was deposited onto pre-patterned FTO coated glass substrates (Thin Film Devices Inc). Sol-gel TiO₂ was prepared by mixing 5 mL of EtOH, two drops of HCl, 125 mL of deionized water, and 375 ml of titanium ethoxide, resulting in a clear solution. The headspace of the vial was filled with nitrogen, and the solution was stirred for 48 hours and then kept in the freezer until use. The sol-gel was spin-cast at 3000 rpm for 20 s and annealed at 115°C for 10 min and 450°C for 30 min. The CsPbI₃ QD film was deposited as noted above. A spiro-OMeTAD hole-transport layer was spin-cast at 5000 RPM from a solution consisting of 72.3 mg of spiro-OMeTAD, 1mL of chlorobenzene, 28.8 μL of 4-TBP, and 17.5 μL of Li-TFSI solution (520 mg Li-TFSI in 100 μL acetonitrile).⁶ A 15 nm layer of MoO₃ was thermally evaporated at a rate of 0.1-0.5 Å/s at base pressures of 2.7E-7 torr. Finally, a 200 nm Al layer was thermally evaporated at a rate of 0.5-2.0 Å/s. *J/V* curves were developed by testing the devices at 1 sun.

Time-resolved photoluminescence measurements

Time-resolved photoluminescence (TRPL) data was measured following excitation using a pulsed excitation source consisting of a supercontinuum fiber laser (Fianium, SC-450-PP) operating at 2 MHz coupled to an acousto-optic tuning filter (Fianium AOTF-Dual) for wavelength selection. The excitation wavelength was chosen depending on the bandgap of the PQDs. The PQD emission was routed to a visible streak camera (Hamamatsu C10910-04) coupled to a spectrograph, and time-resolved spectra were collected over a wavelength range determined to cover the entire PQD emission spectrum. In the TRPL streak camera system, the instrument response function (IRF) depends on the selected time window, but in all cases the IRF was significantly shorter than the measured PL decay.

Time-resolved microwave conductivity measurements

Time-resolved microwave conductivity (TRMC) is a pump-probe technique that can be used to measure the photoconductance of a film without the need for charge collection at electrical contacts.^{7,8}

PQD films were prepared on quartz substrates pre-cut to fill the cross-section of an X-band waveguide (ca. 10.2 mm \times 22.8 mm). This sample is placed in a microwave cavity at the end of the X-band waveguide operating at ca. 9 GHz, and is photoexcited through a grid with a ca. 5 ns laser pulse from an optical parametric oscillator (OPO) pumped by the third harmonic of an Nd:YAG laser operating at 10 Hz. The relative change of the microwave power reflected from the microwave cavity, P , was recorded and is due to absorption of the microwave probe by photoinduced free electrons and holes in the sample, and can be related to the photoconductivity by $\Delta P/P = -K\Delta G$, where the calibration factor K is experimentally determined individually for each sample. Taking into account that photoexcitation results in pairs of electrons and holes, the peak photoconductance can be expressed as:

$$\Delta G = bq_e I_0 F_A (\beta \Sigma \mu) \quad (\text{S.E.1})$$

where q_e is the elementary charge, $\beta = 2.2$ is the geometric factor for the X-band waveguide used, I_0 is the incident photon flux, F_A the fraction of light absorbed at the excitation wavelength, ϕ is the quantum efficiency of free carrier generation per photon absorbed, and $\Sigma\mu$ is the sum of the mobilities of electrons and holes.

Eq. (S1) is used to evaluate the quantum efficiency of free carrier generation per photon absorbed, multiplied by the local mobility of free carriers. These quantities can often be correlated with materials properties or processing conditions, to yield structure-function relationships related to free carrier generation and transport. Although the photoconductance decay after the end of the laser pulse is also a useful tool for the characterization of free carrier decay mechanisms by recombination and trapping, this is beyond the scope of this study. Here, we employ a simple bi-exponential fit of the photoconductivity decay transients, and the average carrier lifetime was calculated according to the equation: $\tau_{\text{avg}} = (A_0\tau_0 + A_1\tau_1)/(A_0 + A_1)$.

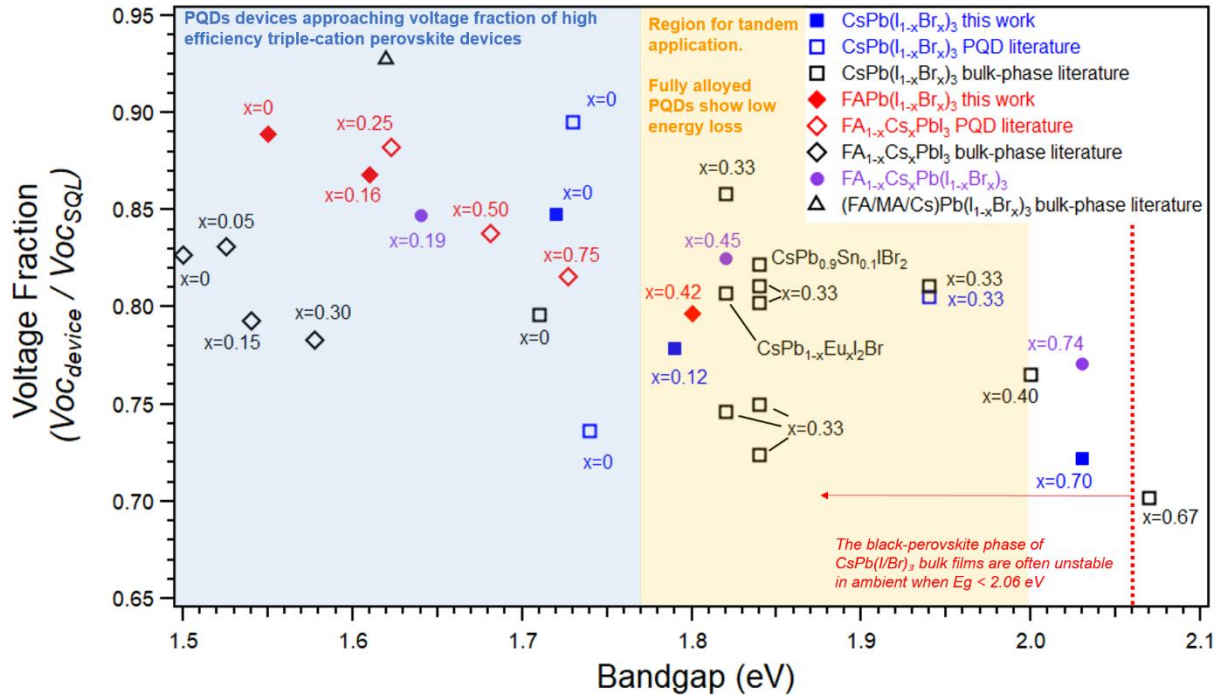


Figure S1. Comparison of experimental PQD PV voltage fraction to literature. Citations for this figure are found at the end of the Supplementary Information. ^{4,9–25}

Table S1. Device metrics for devices shown in Figure 2 of main text

<u>Br comp</u>	<u>Voc</u> <u>(V)</u>	<u>Jsc</u> <u>(mA/cm²)</u>	<u>FF</u>	<u>PCE (%)</u> <u>Reverse scan</u>
0% Br	1.18	16.27	0.73	14.17
8% Br	1.13	14.99	0.60	10.39
13% Br	1.08	10.36	0.47	5.32

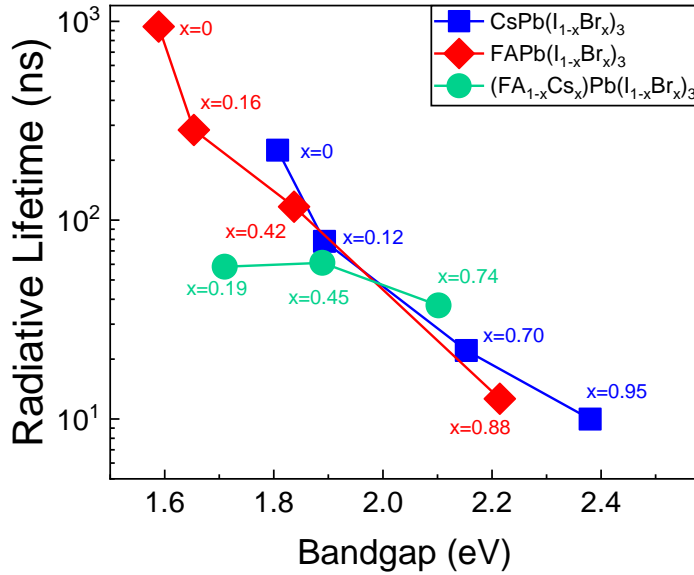


Figure S2. Radiative lifetime of entire PQD sample set.

$$\tau_{rad} = \frac{\phi}{\tau} \quad (\text{S.E.2})$$

Equation S.E.2 shows how to calculate radiative lifetime (τ_{rad}) using measured fluorescence lifetime (τ) and photoluminescence quantum yield (ϕ). Rhodamine 6G was used to estimate relative quantum yield of the $\text{CsPb}(\text{I}_{0.3}\text{Br}_{0.7})_3$ sample because of the compatibility of the absorption and emission spectra. The PLQY of the remainder of the samples were estimated by comparing integrated PL spectra. While relative PLQY measurements, such as this, typically involve some sort of error range, we believe the trend of radiative lifetime versus bandgap and bromine content to be accurate as shown in Figure S4.

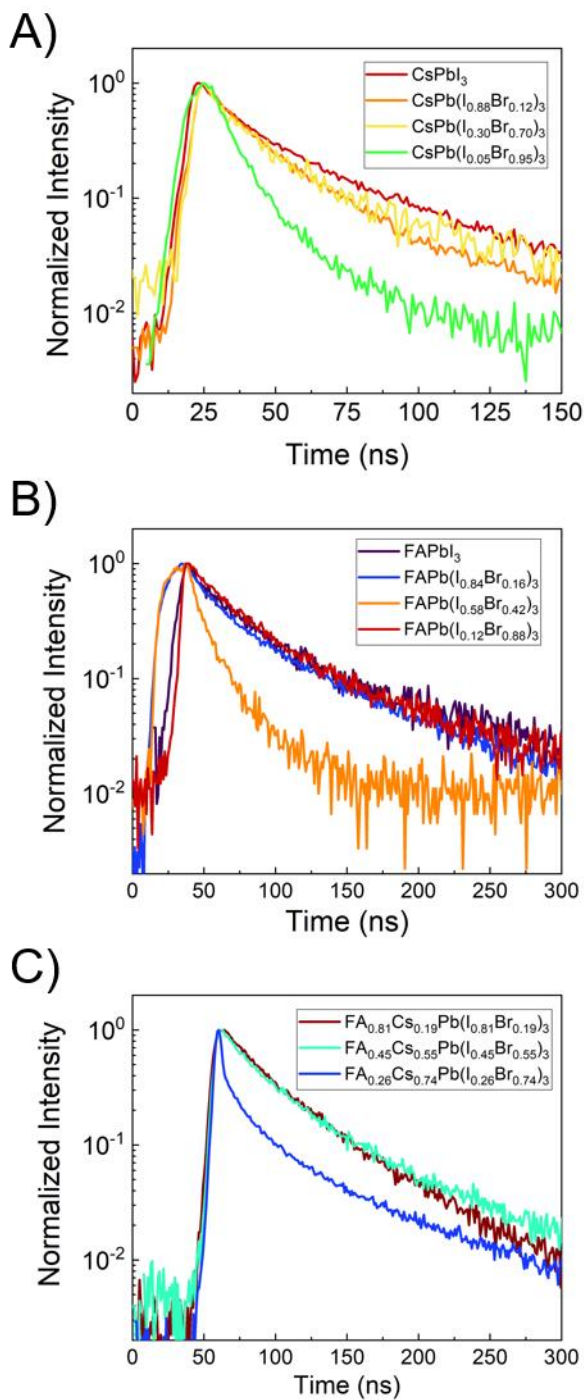


Figure S3. TRPL transients of A) CsPb(I_{1-x}Br_x)₃, B) FAPb(I_{1-x}Br_x)₃, and C) FA_{1-x}Cs_xPb(I_{1-x}Br_x)₃ colloidal PQDs used in devices and for TRMC measurements.

Table S2. Bi-exponential fit parameters extracted from the TRPL decays and used to calculate the intensity-weighted average PL lifetime.

Sample	x	Component 1		Component 2		$\tau_{\text{avg.}}$ (ns)
		τ_1 (ns)	Y ₁ (%)	τ_2 (ns)	Y ₂ (%)	
FAPb(I_{1-x}Br_x)₃	0	23.3	33.4	81.6	66.6	62.1
	0.16	20.3	31.6	84.6	68.4	64.3
	0.42	28.7	42.3	89.6	57.7	63.8
	0.88	6.9	38.2	25.7	61.8	18.5
	1	10.9	73.7	25.3	26.3	14.7
CsPb(I_{1-x}Br_x)₃	0	17.6	39.0	61.6	61.0	44.5
	0.12	14.3	50.3	45.2	49.7	29.7
	0.7	13.3	41.7	41.6	58.3	29.8
	0.95	7.1	67.6	31.9	32.4	15.1
(FA_{1-x}Cs_x)Pb(I_{1-x}Br_x)₃	0.19	23.9	37.4	60.9	62.6	47.0
	0.45	22.3	33.6	72.0	66.4	55.3
	0.6	16.9	31.7	84.5	68.3	63.1

Table S3. Tabulated device metrics for all PQD devices

<u>Composition</u>	<u>Device bandgap (eV)</u>	<u>Voc (V)</u>	<u>Jsc (mA/cm²)</u>	<u>FF</u>	<u>PCE (%)</u>
CsPbI ₃	1.72	1.06	14.40	0.75	11.41
		1.00	14.09	0.77	10.82
		1.01	13.98	0.77	10.91
		1.00	13.97	0.77	10.76
		1.00	13.88	0.79	10.96
		1.05	14.23	0.75	11.13
		1.00	13.56	0.77	10.46
		1.00	13.75	0.77	10.55
		0.98	13.35	0.78	10.21
		1.17	15.80	0.67	12.50
		1.10	15.84	0.67	11.64
		1.17	15.72	0.68	12.51
		1.20	16.37	0.75	14.74
		1.17	15.55	0.70	12.72
		1.11	15.57	0.66	11.41
		1.12	16.07	0.72	12.98
		1.06	15.83	0.58	9.68
		1.09	13.59	0.64	9.42
		1.13	14.44	0.66	10.82
		1.09	13.95	0.67	10.20
		1.12	13.51	0.71	10.78
		1.14	15.10	0.60	10.25
		1.17	14.83	0.61	10.63
		1.10	14.72	0.60	9.78
		1.11	13.99	0.63	9.78
		1.16	14.93	0.64	11.09
		1.10	14.93	0.59	9.67
1.12	14.04	0.64	10.04		
1.17	12.94	0.64	9.71		
CsPb(I _{0.88} Br _{0.12}) ₃	1.79	1.12	11.43	0.60	7.67
		1.10	11.29	0.62	7.74
		1.10	11.07	0.63	7.70
		1.07	11.02	0.62	7.28
		1.10	10.99	0.65	7.81
		1.14	11.83	0.57	7.70
		1.12	11.32	0.62	7.84
		1.14	11.64	0.61	8.08
1.11	11.56	0.60	7.67		

		1.14	11.61	0.62	8.19
		1.16	11.96	0.59	8.14
		1.10	11.68	0.58	7.41
		1.08	11.51	0.58	7.16
		1.07	11.43	0.57	6.98
		1.06	11.33	0.56	6.74
CsPb(I _{0.3} Br _{0.7}) ₃	2.03	1.16	6.30	0.53	3.87
		1.17	5.90	0.54	3.74
		1.16	6.45	0.46	3.41
		1.24	1.41	0.68	1.20
		1.23	1.35	0.67	1.11
		1.23	1.30	0.69	1.10
		1.23	1.33	0.68	1.11
CsPb(I _{0.05} Br _{0.95}) ₃	2.25	1.39	2.36	0.59	1.92
		1.28	2.25	0.58	1.67
		1.22	1.90	0.60	1.39
		1.28	2.18	0.58	1.61
		1.26	2.34	0.57	1.68
		1.24	2.03	0.54	1.37
		1.31	2.43	0.59	1.86
		1.30	2.51	0.58	1.88
		1.29	2.37	0.57	1.75
		1.18	2.09	0.54	1.34
FAPbI ₃	1.55	1.08	15.19	0.64	10.57
		1.08	15.35	0.66	10.85
		1.09	15.52	0.63	10.54
		1.07	15.45	0.65	10.70
		1.08	15.44	0.65	10.92
		1.12	14.73	0.66	10.83
		1.08	14.71	0.73	11.60
		1.09	14.35	0.68	10.54
		1.09	14.50	0.68	10.75
		1.09	13.61	0.80	11.96
FAPb(I _{0.84} Br _{0.16}) ₃	1.61	1.14	15.21	0.65	11.43
		1.11	15.02	0.65	10.99
		1.11	14.36	0.66	10.50
		1.10	14.72	0.64	10.34
		1.11	13.90	0.66	10.17
		1.10	12.93	0.63	9.04
		1.08	13.18	0.65	9.34
		1.06	12.53	0.57	7.67
		1.07	12.09	0.64	8.40
		1.06	11.99	0.62	7.90

FAPb(I _{0.58} Br _{0.42}) ₃	1.80	1.18	10.56	0.54	6.77
		1.18	11.03	0.61	7.97
		1.19	11.09	0.62	8.21
		1.18	11.07	0.63	8.18
		0.44	9.70	0.38	1.60
FA _{0.81} Cs _{0.19} Pb(I _{0.81} Br _{0.19}) ₃	1.64	1.02	12.26	0.55	6.89
		1.05	11.71	0.49	6.07
		0.43	11.31	0.30	1.45
		1.05	11.42	0.47	5.68
		1.05	11.71	0.53	6.47
		1.14	12.7	0.6	8.73
		1.15	12.82	0.64	9.52
		1.11	12.56	0.59	8.27
		1.14	12.87	0.59	8.66
		1.08	12.53	0.57	7.73
		1.1	12.77	0.56	7.9
		1.14	12.54	0.62	8.83
		1.11	12.31	0.58	7.96
		1.14	12.61	0.64	9.19
		1.13	12.52	0.62	8.76
		1.16	12.31	0.62	8.81
		1.17	12.47	0.63	9.16
		1.16	12.76	0.58	8.63
		1.18	12.82	0.65	9.86
		1.10	12.07	0.52	6.85
1.17	11.51	0.55	7.33		
1.18	12.31	0.60	8.74		
1.18	12.46	0.60	8.85		
1.18	12.48	0.61	8.94		
1.18	12.86	0.63	9.59		
FA _{0.55} Cs _{0.45} Pb(I _{0.55} Br _{0.45}) ₃	1.82	1.25	8.75	0.49	5.30
		1.21	9.48	0.50	5.80
		1.21	9.09	0.51	5.55
		1.21	9.83	0.51	6.13
		1.20	9.23	0.50	5.60
		1.22	9.95	0.55	6.75
		1.24	9.91	0.54	6.58
		1.23	9.2	0.5	5.67
		1.24	9.15	0.51	5.81
		1.25	9.93	0.6	7.41
		1.17	9.95	0.56	6.55
		1.23	10.98	0.56	7.57
		1.19	9.27	0.51	5.63



2.03

1.24	11.07	0.6	8.23
1.23	10.39	0.57	7.31
1.24	10.51	0.6	7.9
1.22	10.3	0.51	6.37
1.24	10.68	0.58	7.67
1.26	9.71	0.61	7.42
1.27	10.09	0.60	7.64
1.25	9.81	0.57	6.99
1.26	10.22	0.58	7.45
1.26	10.37	0.59	7.66
1.25	10.48	0.58	7.65
1.21	9.09	0.55	6.04
1.27	9.15	0.54	6.33
1.22	8.79	0.53	5.63
1.16	0.03	0.12	0.00
1.16	10.11	0.48	5.61
1.20	9.98	0.52	6.20
1.16	10.31	0.51	6.05
1.13	10.30	0.44	5.12
1.18	9.57	0.48	5.46
1.2	10.4	0.49	6.13
1.20	5.23	0.49	3.09
1.29	5.71	0.49	3.63
1.18	5.50	0.50	3.23
1.24	4.42	0.46	2.52
1.24	4	0.45	2.21
1.22	3.9	0.45	2.16
1.23	3.49	0.45	1.93
1.29	3.89	0.46	2.29
1.22	3.43	0.44	1.85
1.22	4.33	0.47	2.51
1.24	3.33	0.46	1.89
1.27	4.28	0.46	2.5
1.15	4.06	0.43	2.02
1.1	3.66	0.48	1.95
1.2	2.59	0.48	1.48
1.2	2.49	0.47	1.41
1.2	2.22	0.48	1.28
1.26	1.86	0.52	1.21
1.24	1.22	0.53	0.80
1.19	0.97	0.52	0.60
1.17	1.12	0.54	0.71

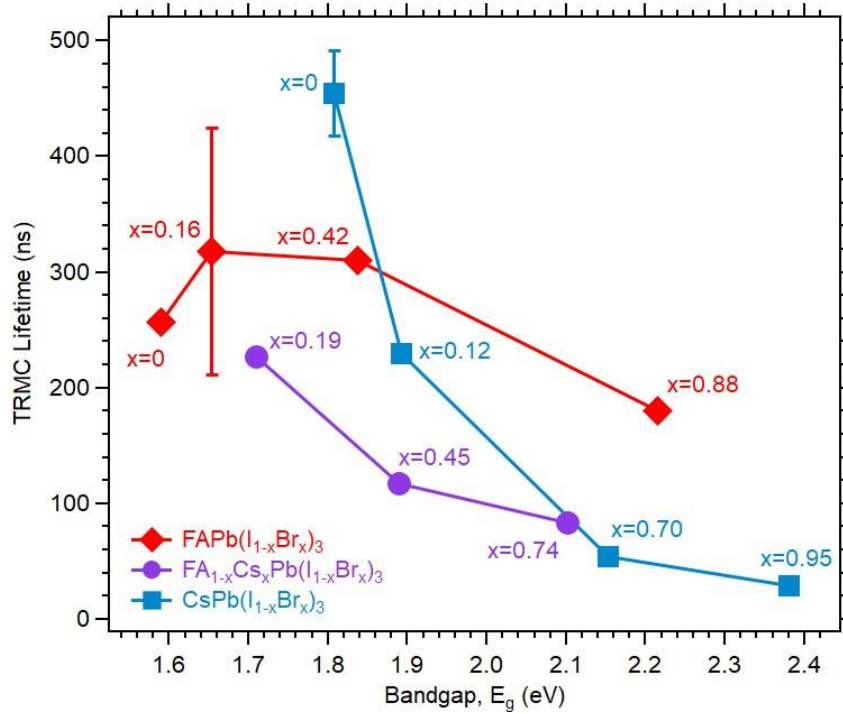


Figure S4. TRMC lifetime versus bandgap for all PQD film samples

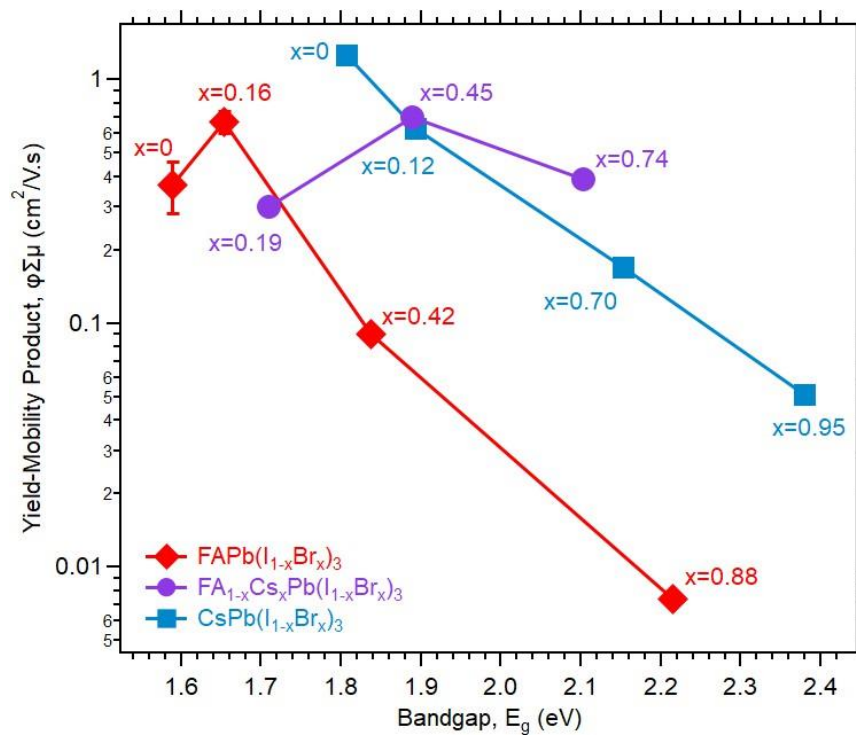


Figure S5. Yield-mobility product versus bandgap for all PQD film samples

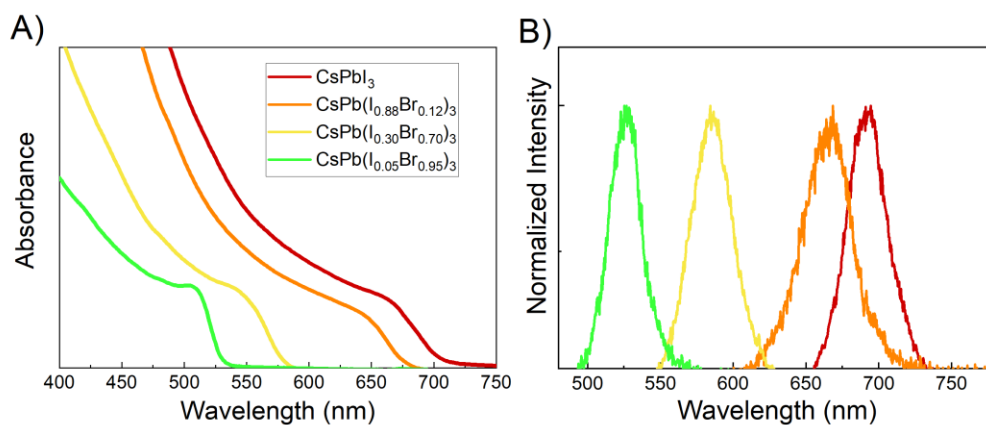


Figure S6. A) absorbance of CsPb(I_{1-x}Br_x)₃ PQD samples used in devices and TRMC measurements, B) photoluminescence spectra of CsPb(I_{1-x}Br_x)₃ PQD samples used in devices and TRMC measurements.

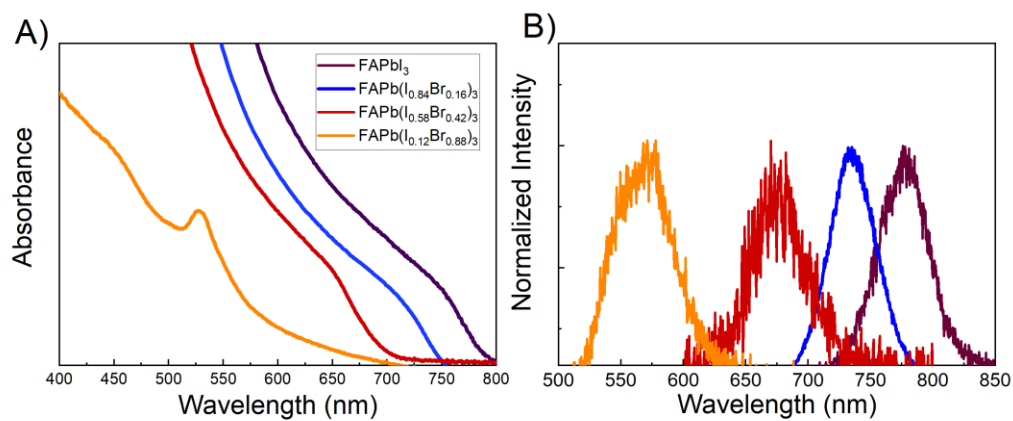


Figure S7. A) absorbance of FAPb(I_{1-x}Br_x)₃ PQD samples used in devices and TRMC measurements, B) photoluminescence spectra of FAPb(I_{1-x}Br_x)₃ PQD samples used in devices and TRMC measurements.

References

- (1) Protesescu, L.; Yakunin, S.; Bodnarchuk, M. I.; Krieg, F.; Caputo, R.; Hendon, C. H.; Yang, R. X.; Walsh, A.; Kovalenko, M. V. Nanocrystals of Cesium Lead Halide Perovskites (CsPbX_3 , X = Cl, Br, and I): Novel Optoelectronic Materials Showing Bright Emission with Wide Color Gamut. *Nano Letters* **2015**, *15* (6), 3692–3696. <https://doi.org/10.1021/nl5048779>.
- (2) Swarnkar, A.; Marshall, A. R.; Sanhira, E. M.; Chernomordik, B. D.; Moore, D. T.; Christians, J. A.; Chakrabarti, T.; Luther, J. M. Quantum Dot-Induced Phase Stabilization of -CsPbI_3 Perovskite for High-Efficiency Photovoltaics. *Science* **2016**, *354* (6308), 92–95. <https://doi.org/10.1126/science.aag2700>.
- (3) Protesescu, L.; Yakunin, S.; Bodnarchuk, M. I.; Bertolotti, F.; Masciocchi, N.; Guagliardi, A.; Kovalenko, M. V. Monodisperse Formamidinium Lead Bromide Nanocrystals with Bright and Stable Green Photoluminescence. *Journal of the American Chemical Society* **2016**, *138* (43), 14202–14205. <https://doi.org/10.1021/jacs.6b08900>.
- (4) Hazarika, A.; Zhao, Q.; Gauding, E. A.; Christians, J. A.; Dou, B.; Marshall, A. R.; Moot, T.; Berry, J. J.; Johnson, J. C.; Luther, J. M. Perovskite Quantum Dot Photovoltaic Materials beyond the Reach of Thin Films: Full-Range Tuning of A-Site Cation Composition. *ACS Nano* **2018**, *12*, 10327–10337. <https://doi.org/10.1021/acsnano.8b05555>.
- (5) Wheeler, L. M.; Sanhira, E. M.; Marshall, A. R.; Schulz, P.; Suri, M.; Anderson, N. C.; Christians, J. A.; Nordlund, D.; Sokaras, D.; Kroll, T.; et al. Targeted Ligand-Exchange Chemistry on Cesium Lead Halide Perovskite Quantum Dots for High-Efficiency Photovoltaics. *Journal of the American Chemical Society* **2018**, *140* (33), 10504–10513. <https://doi.org/10.1021/jacs.8b04984>.
- (6) Saliba, M.; Matsui, T.; Seo, J.-Y.; Domanski, K.; Correa-Baena, J.-P.; Nazeeruddin, M. K.; Zakeeruddin, S. M.; Tress, W.; Abate, A.; Hagfeldt, A.; et al. Cesium-Containing Triple Cation Perovskite Solar Cells: Improved Stability, Reproducibility and High Efficiency. *Energy & Environmental Science* **2016**, *9* (6), 1989–1997. <https://doi.org/10.1039/C5EE03874J>.
- (7) Savenije, T. J.; Ferguson, A. J.; Kopidakis, N.; Rumbles, G. Revealing the Dynamics of Charge Carriers in Polymer:Fullerene Blends Using Photoinduced Time-Resolved Microwave Conductivity. *The Journal of Physical Chemistry C* **2013**, *117* (46), 24085–24103. <https://doi.org/10.1021/jp406706u>.
- (8) Reid, O. G.; Moore, D. T.; Li, Z.; Zhao, D.; Yan, Y.; Zhu, K.; Rumbles, G. Quantitative Analysis of Time-Resolved Microwave Conductivity Data. *Journal of Physics D: Applied Physics* **2017**, *50* (49), 493002. <https://doi.org/10.1088/1361-6463/aa9559>.
- (9) Ghosh, D.; Ali, Md. Y.; Chaudhary, D. K.; Bhattacharyya, S. Dependence of Halide Composition on the Stability of Highly Efficient All-Inorganic Cesium Lead Halide Perovskite Quantum Dot Solar Cells. *Solar Energy Materials and Solar Cells* **2018**, *185*, 28–35. <https://doi.org/10.1016/j.solmat.2018.05.002>.
- (10) Yuan, J.; Zhang, L.; Bi, C.; Wang, M.; Tian, J. Surface Trap States Passivation for High-Performance Inorganic Perovskite Solar Cells. *Sol. RRL* **2018**, *2* (10), 1800188. <https://doi.org/10.1002/solr.201800188>.
- (11) Christodoulou, S.; Di Stasio, F.; Pradhan, S.; Stavrinadis, A.; Konstantatos, G. High-Open-Circuit-Voltage Solar Cells Based on Bright Mixed-Halide CsPbBrI_2 Perovskite

- Nanocrystals Synthesized under Ambient Air Conditions. *The Journal of Physical Chemistry C* **2018**, *122* (14), 7621–7626. <https://doi.org/10.1021/acs.jpcc.8b01264>.
- (12) Zhang, Q.; Zhu, W.; Chen, D.; Zhang, Z.; Lin, Z.; Chang, J.; Zhang, J.; Zhang, C.; Hao, Y. Light Processing Enables Efficient Carbon-Based, All-Inorganic Planar CsPbI₂Br₂ Solar Cells with High Photovoltages. *ACS Appl. Mater. Interfaces* **2019**, *11* (3), 2997–3005. <https://doi.org/10.1021/acsami.8b17839>.
- (13) Zhang, L.; Li, B.; Yuan, J.; Wang, M.; Shen, T.; Huang, F.; Wen, W.; Cao, G.; Tian, J. High-Voltage-Efficiency Inorganic Perovskite Solar Cells in a Wide Solution-Processing Window. *J. Phys. Chem. Lett.* **2018**, *9* (13), 3646–3653. <https://doi.org/10.1021/acs.jpcclett.8b01553>.
- (14) Zhang, J.; Hodes, G.; Jin, Z.; Liu, S. All-Inorganic CsPbX₃ Perovskite Solar Cells: Progress and Prospects. *Angew. Chem. Int. Ed.* **2019**. <https://doi.org/10.1002/anie.201901081>.
- (15) Yu, B.; Zhang, H.; Wu, J.; Li, Y.; Li, H.; Li, Y.; Shi, J.; Wu, H.; Li, D.; Luo, Y.; et al. Solvent-Engineering toward CsPb(I_xBr_{1-x})₃ Films for High-Performance Inorganic Perovskite Solar Cells. *J. Mater. Chem. A* **2018**, *6* (40), 19810–19816. <https://doi.org/10.1039/C8TA07968D>.
- (16) Xiang, W.; Wang, Z.; Kubicki, D. J.; Tress, W.; Luo, J.; Prochowicz, D.; Akin, S.; Emsley, L.; Zhou, J.; Dietler, G.; et al. Europium-Doped CsPbI₂Br for Stable and Highly Efficient Inorganic Perovskite Solar Cells. *Joule* **2019**, *3* (1), 205–214. <https://doi.org/10.1016/j.joule.2018.10.008>.
- (17) Wang, Y.; Zhang, T.; Xu, F.; Li, Y.; Zhao, Y. A Facile Low Temperature Fabrication of High Performance CsPbI₂Br All-Inorganic Perovskite Solar Cells. *Sol. RRL* **2018**, *2* (1), 1700180. <https://doi.org/10.1002/solr.201700180>.
- (18) Wang, P.; Zhang, X.; Zhou, Y.; Jiang, Q.; Ye, Q.; Chu, Z.; Li, X.; Yang, X.; Yin, Z.; You, J. Solvent-Controlled Growth of Inorganic Perovskite Films in Dry Environment for Efficient and Stable Solar Cells. *Nat Commun* **2018**, *9* (1), 2225. <https://doi.org/10.1038/s41467-018-04636-4>.
- (19) Sutton, R. J.; Eperon, G. E.; Miranda, L.; Parrott, E. S.; Kamino, B. A.; Patel, J. B.; Hörlantner, M. T.; Johnston, M. B.; Haghighirad, A. A.; Moore, D. T.; et al. Bandgap-Tunable Cesium Lead Halide Perovskites with High Thermal Stability for Efficient Solar Cells. *Adv. Energy Mater.* **2016**, *6* (8), 1502458. <https://doi.org/10.1002/aenm.201502458>.
- (20) Sanchez, S.; Christoph, N.; Grobety, B.; Phung, N.; Steiner, U.; Saliba, M.; Abate, A. Efficient and Stable Inorganic Perovskite Solar Cells Manufactured by Pulsed Flash Infrared Annealing. *Adv. Energy Mater.* **2018**, *8* (30), 1802060. <https://doi.org/10.1002/aenm.201802060>.
- (21) Liang, J.; Zhao, P.; Wang, C.; Wang, Y.; Hu, Y.; Zhu, G.; Ma, L.; Liu, J.; Jin, Z. CsPb_{0.9}Sn_{0.1}I₂Br₂ Based All-Inorganic Perovskite Solar Cells with Exceptional Efficiency and Stability. *J. Am. Chem. Soc.* **2017**, *139* (40), 14009–14012. <https://doi.org/10.1021/jacs.7b07949>.
- (22) Li, W.; Rothmann, M. U.; Liu, A.; Wang, Z.; Zhang, Y.; Pascoe, A. R.; Lu, J.; Jiang, L.; Chen, Y.; Huang, F.; et al. Phase Segregation Enhanced Ion Movement in Efficient Inorganic CsPbI₂Br₂ Solar Cells. *Adv. Energy Mater.* **2017**, *7* (20), 1700946. <https://doi.org/10.1002/aenm.201700946>.

- (23) Dong, C.; Han, X.; Zhao, Y.; Li, J.; Chang, L.; Zhao, W. A Green Anti-Solvent Process for High Performance Carbon-Based CsPbI₂Br All-Inorganic Perovskite Solar Cell. *Sol. RRL* **2018**, *2* (9), 1800139. <https://doi.org/10.1002/solr.201800139>.
- (24) Chen, W.; Chen, H.; Xu, G.; Xue, R.; Wang, S.; Li, Y.; Li, Y. Precise Control of Crystal Growth for Highly Efficient CsPbI₂Br Perovskite Solar Cells. *Joule* **2019**, *3* (1), 191–204. <https://doi.org/10.1016/j.joule.2018.10.011>.
- (25) Correa-Baena, J-P; Tress, W; Domanski, K; Ankari, E; Turren-Cruz, S; Roose, B; Boix, P; Gratzel, M; Saliba, M; Abate, A; Hagfeldt, A. Identifying and suppressing interfacial recombination to achieve high open-circuit voltage in perovskite solar cells. *Energ & Environ Sci*. **2017**. *10*, 1207-1212